

Cite this: *Soft Matter*, 2015, 11, 1078

Shape-controlled orientation and assembly of colloids with sharp edges in nematic liquid crystals

Daniel A. Beller,^{*a} Mohamed A. Gharbi^{ab} and Iris B. Liu^b

The assembly of colloids in nematic liquid crystals *via* topological defects has been extensively studied for spherical particles, and investigations of other colloid shapes have revealed a wide array of new assembly behaviors. We show, using Landau-de Gennes numerical modeling, that nematic defect configurations and colloidal assembly can be strongly influenced by fine details of colloid shape, in particular the presence of sharp edges. For cylinder, microbullet, and cube colloid geometries, we obtain the particles' equilibrium alignment directions and effective pair interaction potentials as a function of simple shape parameters. We find that defects pin at sharp edges, and that the colloid consequently orients at an oblique angle relative to the far-field nematic director that depends on the colloid's shape. This shape-dependent alignment, which we confirm in experimental measurements, raises the possibility of selecting self-assembly outcomes for colloids in liquid crystals by tuning particle geometry.

Received 27th August 2014
Accepted 8th December 2014

DOI: 10.1039/c4sm01910e

www.rsc.org/softmatter

1 Introduction

A promising route toward targeted colloidal self-assembly is to disperse colloids in a nematic liquid crystal, whose elasticity resists the deformations caused by anchoring conditions at the surfaces of the colloids, resulting in forces on the colloids that push them into ordered arrangements such as chains and triangular lattices.^{1–5} Nematic colloidal dispersions are especially interesting because each colloidal particle is accompanied by a topological defect or defects in the liquid crystal that play a key role in the assembly process.^{1,2,6} Spherical colloids have been extensively studied in this context. When the spherical colloid's surface imposes strong homeotropic (normal) anchoring conditions on the nematic director field, the companion defect is either a point-like hedgehog or a linear "Saturn ring" disclination about the equator. Ring disclinations can be manipulated, such as by laser tweezers, to topologically entangle multiple colloids into chains⁷ and knotted structures.⁸ Because the colloidal lengthscale roughly coincides with the wavelengths of visible light, colloidal structures assembled by nematic elasticity and topological defects hold strong potential for photonics applications such as photonic bandgap crystals.^{9–11}

While much of the research on nematic colloidal dispersions has concentrated on spherical colloidal particles, colloidal self-assembly in general is known to depend strongly on the shapes of the colloidal particles. This has

been amply demonstrated in the entropically-driven self-assembly of hard particles^{12–14} and in the capillarity-driven assembly of colloids at fluid interfaces.¹⁵ Recent advances in colloid fabrication techniques, such as photolithography, have enabled fairly precise creation of particles with designed asymmetric shapes as well as surface functionalization.¹⁶ In nematics, a number of recent investigations have begun to explore how defect configuration and assembly behavior change when the particle has a non-spherical geometry, such as rods,¹⁷ spherocylinders,¹⁸ ellipsoids,¹⁹ microbullets (rods with one flat end and one rounded end),²⁰ polygonal platelets,^{21,22} washers,²³ handle-bodies of varying genus,²⁴ and Möbius bands.²⁵ In addition, nontrivial colloid or substrate geometry has been shown to provide elastically attractive or repulsive sites influencing the organization of colloids in the bulk or at an interface.^{23,26–28}

While these investigations have found a variety of phenomena resulting from gross changes to the colloid shape, or even topology, as compared to spheres, it is important to also keep in mind that fine details of colloid shape can play a surprisingly important role. In particular, sharp edges often act as pinning sites for nematic defects because of the elastic strain that they impose through a large variation in the anchoring direction over a small region.^{26,29,30} (An abrupt change in anchoring chemistry from degenerate planar to homeotropic has a similar pinning effect.)^{31,32} Therefore, a rod-like colloid with rounded ends, such as a spherocylinder or ellipse, may behave quite differently from a cylinder. These distinctions prompt caution but also suggest a path to tuning colloidal assembly properties by varying the details of colloid shape.

^aDepartment of Physics and Astronomy, University of Pennsylvania, Philadelphia, Pennsylvania 19104, USA. E-mail: dbeller8@gmail.com

^bDepartment of Chemical and Biomolecular Engineering, University of Pennsylvania, Philadelphia, Pennsylvania 19104, USA

In this paper, we investigate the topological defect configurations and assembly properties of colloids with sharp edges, in the shapes of cylinders, microbullets, and cubes. We focus primarily on the case of colloids with strong homeotropic anchoring confined in thin planar cells, in the regime where the companion topological defect is a disclination ring (valid for colloids of small size³³ and/or under strong confinement³⁴). Through Landau-de Gennes numerical modeling, we show that the edges of these shapes result in significantly different defect ring configurations than those seen with smooth shapes such as spheres and ellipsoids. The quadrupolar symmetry of the smooth rods' Saturn ring configuration is lost for shapes with edges; instead, defect rings pin at portions of the edges. As a result, cylinders and microbullets orient at oblique angles relative to the far-field nematic director, an effect not seen at equilibrium in smooth rods such as spherocylinders¹⁸ or ellipsoids.¹⁹ This oblique angle increases with the aspect ratio of the colloid, as we confirm with experimental observations, demonstrating tunable colloidal alignment and interactions through particle geometry.

In addition, the disclination configuration spontaneously breaks a reflection symmetry or symmetries, implying multi-stable colloidal orientations. We find that this multistability strongly affects not only colloidal pair interactions but also the defect behavior on individual colloids, which may exhibit sudden jumps between defect configurations in response to an applied torque. Our results highlight the importance of details of particle geometry in relation to topological defects and colloidal interactions, and suggest new routes toward complex and multi-stable self-assembled structures in nematic colloidal dispersions.

2 Numerical approach

We study the nematic liquid crystal using Landau-de Gennes (LdG) numerical modeling.³⁵ The nematic state is represented as a traceless symmetric tensor field $\mathbf{Q}(\vec{x})$, which in a uniaxial nematic with director \vec{n} satisfies $Q_{ij} = \frac{3}{2}S\left(n_i n_j - \frac{1}{3}\delta_{ij}\right)$. The leading eigenvalue S is the nematic degree of order, and we visualize defects as isosurfaces where S falls to 3/4 of its bulk value S_0 in an undistorted nematic, except where otherwise indicated. The LdG free energy in the single-elastic constant limit,

$$F_{\text{LdG}} = \int dV \left[\frac{1}{2} A \text{tr}(\mathbf{Q}^2) + \frac{1}{3} B \text{tr}(\mathbf{Q}^3) + \frac{1}{4} C (\text{tr}(\mathbf{Q}^2))^2 + \frac{L}{2} \frac{\partial Q_{ij}}{\partial x_k} \frac{\partial Q_{ij}}{\partial x_k} \right], \quad (1)$$

is minimized numerically in a finite difference scheme on a regular cubic mesh with grid spacing 4.5 nm, using a conjugate gradient algorithm from the ALGLIB package (<http://www.alglib.net>). We take from ref. 35 the typical values for the material constants of the commonly used nematic liquid crystal 5CB: $A = -0.172 \times 10^6 \text{ J m}^{-3}$, $B = -2.12 \times 10^6 \text{ J m}^{-3}$, $C = 1.73 \times 10^6 \text{ J m}^{-3}$. We set the elastic constant $L = 8 \times 10^{-12} \text{ N}$ to

correspond to a Frank elastic constant $K = L9S_0^2/2 \approx 1 \times 10^{-11} \text{ N}$ roughly matching the elastic constants of 5CB.³⁶ We do not include a surface energy term because we study the limit of infinitely strong anchoring, where \mathbf{Q} is held fixed at the boundaries to give a fixed boundary director.³⁷ (We have checked that replacing this assumption with the presence of a Nobili-Durand surface anchoring term $W \int dA \text{tr}((\mathbf{Q} - \mathbf{Q}^s)^2)$, where \mathbf{Q}^s is the \mathbf{Q} favored by the surface, in F_{LdG} does not change the results significantly for experimentally realistic anchoring strength W in the strong anchoring regime.)

The top and bottom boundaries of the rectangular cell have oriented planar anchoring along a uniform direction, the “rubbing direction”, which defines the bulk far-field director \vec{n}_0 . At the sides of the box, we use free boundary conditions, eschewing periodic boundary conditions to ensure that a colloid does not interact with its periodic images. The colloid, with infinitely strong homeotropic anchoring, is placed at the mid-height of the cell, and its orientation is held fixed while the nematic configuration $\mathbf{Q}(\vec{x})$ is relaxed. The initial condition consists of a uniform uniaxial nematic with director $\vec{n} = \vec{n}_0$ everywhere except the boundaries; we have checked in several instances that random initial conditions produce either the same states or metastable states of higher energy.

When studying the effects of colloid shapes with edges, we have to take care not to make the modeled edges *too* sharp because perfectly sharp edges introduce an unrealistic ambiguity into the director field: the rotation of the director through $\pm 90^\circ$ can be accomplished through either splay or bend, which have equal energy in the one-elastic-constant approximation. Because the colloidal edges are expected to be rounded in a convex way at least at the molecular scale, the splay configuration is more realistic. In order to obtain this configuration, we round the edges of numerically modeled cylindrical colloids using the “superegg” equation,

$$\left(\frac{x^2 + y^2}{b^2}\right)^p + \left(\frac{z^2}{a^2}\right)^p = 1. \quad (2)$$

Here the coordinate frame has been rotated so that the colloid long axis points along the z direction; b is the colloid radius; a is half the colloid length; and p is a parameter we refer to as the “sharpness” of the shape, interpolating between an ellipsoid at $p = 1$ and a right circular cylinder as $p \rightarrow \infty$. We treat p as an adjustable shape parameter controlling the degree to which curvature is concentrated in edges. To model microbullets, only the half of the colloid opposite the hemispherical cap is given the superegg shape; the other half is spherocylindrical, with no edges.

Similarly, to model colloidal cubes, we round the edges using a special case of the superellipsoid equation,

$$x^{2p} + y^{2p} + z^{2p} = a^{2p}. \quad (3)$$

Here, p interpolates the shape between a sphere of radius a at $p = 1$ and a cube of side length $2a$ as $p \rightarrow \infty$ (for simplicity, we do not vary the aspect ratio for this shape).

3 Colloidal cylinders and microbullets: shape-controlled orientation

Before presenting our results, we recall the known behavior of homeotropic spherical particles in a nematic. A spherical colloid imposing strong homeotropic anchoring on the director field at the colloid's surface acts as a radial hedgehog, and is thus accompanied by a stable topological defect to ensure zero total topological charge.³⁸ This companion defect can be either a hyperbolic point hedgehog or a "Saturn ring" disclination of unit topological charge.⁶ In the latter case, the ring's stable position is around the equator of the colloid, in the plane orthogonal to the far-field nematic director \vec{n}_0 , and the director field has quadrupolar symmetry.³⁹ For an isolated spherical colloid, the director field in a cross-section transverse to the disclination tangent is that of a 2D nematic disclination with winding number $-1/2$. In the case of a hedgehog defect, the director field has dipolar symmetry, with the hedgehog separated from the colloid center along the \vec{n}_0 direction. Smaller colloid size³³ or stronger confinement³⁴ tends to stabilize the Saturn ring relative to the hedgehog. These sphere-defect pairs self-assemble into chains parallel to \vec{n}_0 in the case of hedgehog defects, and kinked chains making an angle $\sim 73^\circ$ with \vec{n}_0 in the case of Saturn rings.^{2,5} Saturn rings of neighboring colloids may also join into a single disclination ring that entangles pairs or chains of colloids.⁷

For homeotropic colloids that are topologically but not geometrically spheres, such as cubes and cylinders (with edges at least slightly rounded), the same topology applies to the surrounding nematic: each genus-zero colloid is accompanied by a companion defect, either a hedgehog or a disclination ring.^{17,18,37} Colloidal micro-rods have been shown to form chains and bound pairs depending on the types and positions of their defects, which were either a hedgehog near the micro-rod's end or a disclination ring wrapping around the colloid's long axis.¹⁷

Our LdG numerical modeling of rod-like colloids shows that the details of particle shape strongly affect both the defect configuration and the colloids' alignment and assembly. We numerically model homeotropic ellipsoids, cylinders, and microbullets confined in thin cells of thickness three times the colloid diameter, with oriented planar anchoring at the boundaries, and we seek the equilibrium angle ϕ_0 of the rod-like colloid's long axis (assumed to lie in the horizontal plane) relative to the far-field director \vec{n}_0 .

For ellipsoids, we find that the disclination ring wraps around the colloid's long axis, as shown in Fig. 1b, and that the colloid prefers to orient at $\phi = 90^\circ$, with the long axis perpendicular to \vec{n}_0 .¹⁹ The results are markedly different in the case of cylinders. Fig. 1c and d show the defect configuration around a cylinder modeled as a superegg using eqn (2), with sharpness $p = 10$. The disclination ring still wraps around the long axis of the colloid, but something new happens at the sharp edges at the ends of the cylinder: the disclination loop follows an "S"-shaped contour, as viewed from above, with sharp turns to follow one half of the circular edge at one end and the opposite

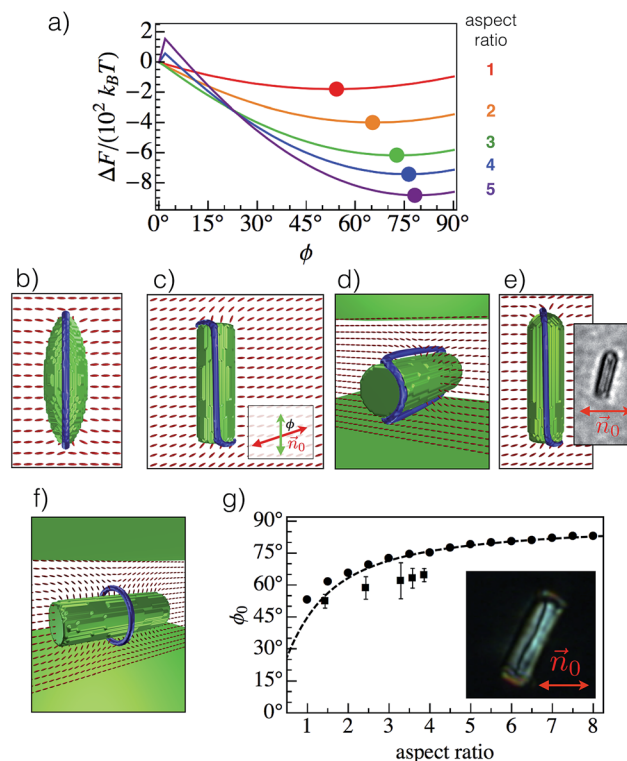


Fig. 1 Rod-like colloids. (a) Free energy of a colloidal cylinder (diameter 90 nm), modeled as a $p = 10$ superegg, in a planar nematic cell (thickness 270 nm) with strong unidirectional planar anchoring. Free energy is plotted as a function of the angle ϕ between the cylinder's long axis and the far-field director \vec{n}_0 , with $\phi = 0$ taken as the $\Delta F = 0$ reference state for each aspect ratio. (b–e) Equilibrium disclination configuration around an ellipsoid (b), a cylinder (c and d), and a microbullet (e), with defects in blue and the director field in red; all have diameter 90 nm, aspect ratio 3, and sharpness $p = 10$. Inset to (e) shows an experimental bright-field optical image of a microbullet of diameter 2 μm and length 10 μm at its equilibrium tilt. (f) An alternative disclination arrangement for cylinders found numerically that is responsible for the sharp peaks in (a) at small ϕ for aspect ratios 4 and 5. (g) Comparison of the energy-minimizing cylinder axis angle ϕ_0 predicted numerically (circles) with experimental data (squares) and the inverse tangent of the aspect ratio (dashed curve). Inset: experimental polarized optical microscopy image of a colloidal cylinder of length 17 μm at its equilibrium oblique tilt ϕ_0 .

half of the circular edge at other end. This defect configuration represents an energetic compromise between the configuration preferred by the ellipsoid and the preference for defects to pin at sharp edges to reduce splay.

As a result of this new defect configuration, the cylinder prefers to orient with its long axis at an oblique angle ϕ_0 relative to \vec{n}_0 , and ϕ_0 increases toward 90° with increasing aspect ratio a/b . Fig. 1a shows the change in free energy as cylinders of various aspect ratios are rotated by an angle ϕ relative to \vec{n}_0 . For aspect ratios $a/b \geq 2$, ϕ_0 is well approximated by $\tan^{-1}(a/b)$, as shown in Fig. 1g, suggesting that (at least heuristically) the energy is minimized when the separation vector between the kinked ends of the disclination lies in the plane perpendicular to \vec{n}_0 . This analytic approximation improves in accuracy as the sharpness p is increased, as shown in Fig. 4b, while the

qualitative trend of ϕ_0 increasing with aspect ratio persists with decreasing p down to $p \approx 2$. For oblate cylinder shapes with aspect ratios below 1 (down to $a/b = 0.25$, the lowest tested), the kinked disclination configuration and oblique colloid orientation remain, but the positive correlation of ϕ_0 with a/b disappears.

An alternative configuration, with the disclination ring encircling the colloid's short axis about its center (Fig. 1f), is also observed at high aspect ratio, but this state only appears when the colloid is constrained to orient at unfavorably small angles ϕ relative to \vec{n}_0 . (Sometimes the ring is localized at one of the cylinder ends instead of about its center.) If the aspect ratio is increased sufficiently, we expect that the defect's core energy per unit length might allow this short-axis disclination ring to eventually overtake the kinked long-axis disclination loop in stability, resulting in alignment of long cylindrical colloids parallel to the far-field director at $\phi = 0$. However, in the numerical results, the kinked long-axis disclination loop remains stable, with $\phi_0 \approx \tan^{-1}(a/b)$, for aspect ratios up to $a/b = 10$, the highest tested.

We find a similar result for microbullets (Fig. 1e). Here, the disclination again wraps around the colloid's long axis and turns sharply to follow half of the circular end. At the rounded end, the disclination is nearly undeflected. The energetically preferred colloidal orientation ϕ_0 is again oblique and increases with increasing aspect ratio. At all aspect ratios tested, ϕ_0 is well approximated simply by the average of $\tan^{-1}(a/b)$ and 90° .

Experimental measurements on colloidal cylinders in the nematic liquid crystal 5CB are in qualitative agreement with these numerical predictions. Colloidal cylinders of diameter 7 μm and varying aspect ratios are fabricated using standard lithographic techniques with SU-8, a negative photoresist. To impose homeotropic anchoring of the nematic at their surfaces, the cylinders are covered with a thin layer of chromium (around 30 nm) then treated with a 3% wt solution of *N,N*-dimethyl-*N*-octadecyl-3-aminopropyltrimethoxysilyl chloride (DMOAP) in a mixture of 90% wt ethanol and 10% wt water. Two glass coverslips, treated with a 1% wt solution of polyvinyl alcohol (PVA) in a mixture of 5% wt ethanol and 95% wt water and rubbed along one direction after heating, are used to create a thin planar cell of thickness approximately 10 μm (fixed using Mylar spacers). A 1% wt dispersion of colloidal cylinders in 5CB is introduced into the LC cells *via* capillarity.

We observe that cylinders with hedgehog companion defects align parallel to \vec{n}_0 , while many cylinders with disclination rings are wrapped by their defects in an approximately straight line along the cylinder axis as viewed from above, consistent with the "S"-shaped contour profile predicted numerically (see inset to Fig. 1g). For the latter configuration, the cylinders are oriented at an oblique angle ϕ_0 between 45° and 90° that increases with the cylinder's aspect ratio (Fig. 1g). We observe a similar oblique ϕ_0 for microbullet colloids with ring defects (see inset to Fig. 1e), fabricated as described in ref. 20. We also note that, in ref. 17, a wide range of micro-rod orientations $35^\circ \lesssim \phi_0 \lesssim 90^\circ$ was reported for a wide range of aspect ratios $1.3 \lesssim a/b \lesssim 4.7$.

Detailed views of the numerically observed director field profile about the disclinations are given in Fig. 2 for a

cylindrical colloid approximated as a spherocylinder of diameter 144 nm, aspect ratio 3, and sharpness $p = 10$. There it is seen that the director profile in a plane perpendicular to the defect tangent is always approximately that of a planar nematic disclination with winding number $-1/2$. This is true on both the approximately straight and approximately semicircular segments of the disclination, as well as the disclination kinks where these different segments meet. On the other hand, the disclination's distance from the colloid surface changes significantly between the different segments. On the approximately straight segments that travel along the cylinder's long axis, the disclination is roughly 18 nm, or about 6 times the nematic correlation length $\xi_N \approx 3.0$ nm, away from the colloid surface, whereas along the semicircular segments along the colloid edges, the distance is about half as great. For spherical colloids, it has previously been found numerically that the distance of the Saturn ring from the colloid surface increases with colloid radius³³ (here we refer to absolute distance, not its ratio to the colloid radius). The variation of defect-colloidal surface separation around a single cylindrical colloid in Fig. 2 suggests that this principle holds for local curvature, as well.

We also observe a dependence of colloid orientation ϕ_0 on aspect ratio when the colloid's anchoring conditions are degenerate planar rather than homeotropic. However, the change in ϕ_0 reverses, now decreasing with increasing aspect ratio (Fig. 3a). In other words, as the aspect ratio increases the colloid long axis orients increasingly toward \vec{n}_0 rather than toward $\hat{z} \times \vec{n}_0$. Here, we use the degenerate planar anchoring potential of Fournier and Galatola⁴⁰ with $W_1 = W_2 = 1.0 \times 10^{-2}$ J m⁻², which is in the strong anchoring regime. The defect structure in this case is a pair of boojums, with +1 winding number in the surface of the colloid, situated on opposing portions of the cylinder's two edges (Fig. 3b and c). The regions of melted nematic signalling the presence of boojums extend somewhat to follow the circular shape of the edge. Comparing to Fig. 1c and d, we see that each boojum sits on the half of the circular edge not followed by the disclination in the case of homeotropic anchoring.

How does our observed oblique colloidal alignment depend on the sharpness of the colloidal particle's edges? In Fig. 4, we

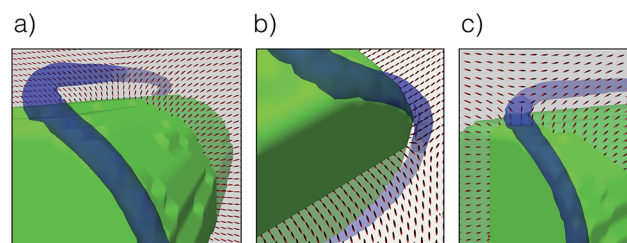


Fig. 2 Detailed view of the director field around a cylindrical colloid. The cylinder in this case is a $p = 10$ spherocylinder with diameter $2b = 144$ nm and aspect ratio $a/b = 3$. The spacing between rods in the director field profile is 4.5 nm, or 1.5 times the nematic correlation length. (a) Director profile in a plane normal to the colloid's long axis, near the colloid's center. (b) Director profile in a plane parallel to the planar boundaries, at one end of the cylinder. (c) Director profile in a plane oblique to the colloid, passing through a kink in the disclination.

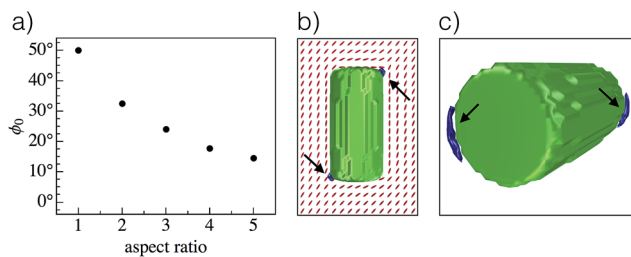


Fig. 3 Equilibrium orientation of cylindrical colloids with strong degenerate planar anchoring. The colloids have diameter $2b = 90$ nm and sharpness parameter $p = 10$. (a) Dependence of equilibrium colloid orientation ϕ_0 on the aspect ratio. (b) Director field and boojum defect structure for a cylinder with aspect ratio 2, viewed from above. For better visibility, the boojums are visualized here as isosurfaces of $S = 0.85 \times S_0$ and indicated with arrows. (c) The same cylinder and its defects viewed from the side, showing that the regions of melted nematic at the boojums (again indicated with arrows) extend along portions of the edges.

numerically vary the sharpness parameter p for cylinders modeled as supereggs, fixing the aspect ratio at 3. The equilibrium long-axis angle ϕ_0 is plotted against R_c/ξ_N in Fig. 4a, where R_c is the radius of curvature of the superegg edge (the minimum radius of curvature of the superellipse cross-section) and $\xi_N \approx 3.0$ nm is the nematic correlation length. As the edge's radius of curvature increases, ϕ_0 increases toward 90° , the value favored by ellipsoids. This increase in ϕ_0 is slower for larger cylinders. However, the same data for ϕ_0 collapses nicely across colloid sizes when plotted against the sharpness parameter p in

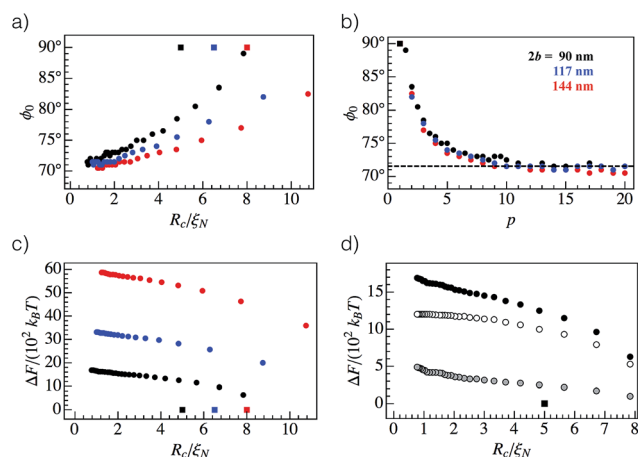


Fig. 4 Effect of colloid edge sharpness: data for cylinders, approximated as supereggs, of aspect ratio $a/b = 3$ and diameter $2b = 90$ nm (black), 117 nm (blue), and 144 nm (red). (a) Equilibrium angle ϕ_0 versus the radius of curvature R_c of the edge (minimum radius of curvature of the superellipse cross-section), in units of the nematic correlation length $\xi_N \approx 3.0$ nm. Square symbols show data for $p = 1$ ellipsoids, where for comparison R_c is taken to be the radius of curvature at the ends. (b) Equilibrium angle ϕ_0 plotted against sharpness parameter p . Dashed line shows analytic approximation $\phi_0 = \tan^{-1}(a/b)$. (c) Free energy compared to that of $p = 1$ ellipsoid (square symbols). (d) For the superegg with diameter 90 nm, the total free energy (black disks), and its bulk (white disks) and elastic (gray disks) free energy components, compared to that of $p = 1$ ellipsoid (black square).

Fig. 4b, rather than against R_c . This shows that the shape, rather than absolute size scale of the edge, determines the colloid's orientation.

The free energy compared to that of the $p = 1$ ellipsoid increases as p increases (decreasing R_c), as shown in Fig. 4c, and unsurprisingly the energy increases faster for larger supereggs. The bulk and elastic components of the free energy (respectively, integrals of the first and second lines of the integrand in eqn (1)) are plotted in Fig. 4d. The bulk component, chiefly the defect core energy, contributes the most to the free energy's dependence on edge sharpness. However, the contribution of the elastic energy component is also significant, and increasing so at larger sharpness (smaller R_c).

Another consequence of the disclination configuration found above is that there are two energetically equivalent ground states: that of Fig. 1c and its mirror image reflected through \vec{n}_0 . We now wish to calculate pair potentials for colloidal cylinders in the thin planar cell geometry, which we will show to depend strongly on whether the two cylinders are in the same or mirror-image configurations.

To begin to understand how the effect of sharp edges on colloids' orientation in turn affects the properties of colloidal assembly, we seek to calculate the energy of pairs of cylindrical colloids. To reduce the number of variables, we fix the orientation of both cylinders in the ground-state orientation of an isolated cylinder.³⁷ The remaining variables are the distance and angle of the cylinders' center-to-center separation, as well as the choice of equivalent or mirror-image ground states for the colloidal pair.

The pair potential for two cylinders in the same ground state is shown in Fig. 5a. These cylinders attract end-to-end, as shown by the decrease in energy with decreasing center-to-center separation distance as the cylinders, oriented at angle ϕ_0 , approach along a separation angle $\phi_{\text{sep}} = \phi_0$ relative to \vec{n}_0 , as illustrated in Fig. 5b(2). This result predicts end-to-end chaining for a series of cylinders in the equivalent ground state orientation. Whether cylinders remain oriented at an angle ϕ_0 relative to \vec{n}_0 after forming a chain is an open question. LdG modeling shows that a chained cylinder pair can slightly lower its energy by fusing the two disclination rings into one, and reorienting the chained cylinders at a larger angle ϕ_0 preferred by a single cylinder of twice the aspect ratio. This suggests cylinders might “untilt” toward $\phi = 90^\circ$ as they assemble into chains. However, there may be a significant energy barrier to such a rearrangement of two disclination loops into one, just as the entangling of spherical colloids requires an input of energy, typically from laser tweezers, to melt the nematic locally.⁷ Meanwhile, the two cylinders in Fig. 5a repel at two angles near $\phi_{\text{sep}} = \phi_0$, corresponding to the situations shown in Fig. 5b(1 and 3) where the approaching sides of the cylinder edges are both with or both without the disclination.

The pair potential changes drastically when the two cylinders are instead in the different, mirror-image states (Fig. 5c). At large distances, the cylinders repel strongly when approaching along a line perpendicular to \vec{n}_0 . However, if the cylinders are forced close enough together, one of the two disclinations switches the side of the cylinder end that it follows, replacing

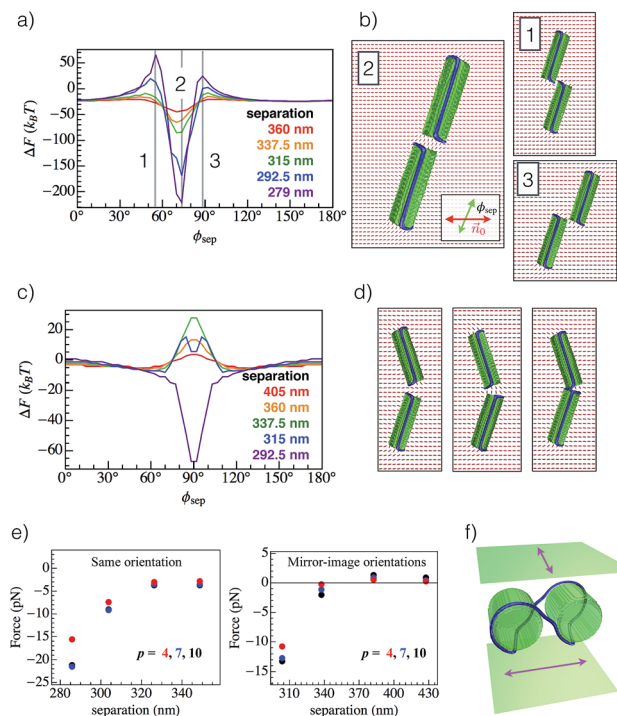


Fig. 5 Interaction of two colloidal cylinders. Both cylinders have diameter $2b = 90$ nm, aspect ratio $a/b = 3$, and sharpness $p = 10$. (a) Pair potential (plus an arbitrary uniform shift) for two cylinders held at the same single-particle-equilibrium orientation, as a function of their separation angle ϕ_{sep} relative to \vec{n}_0 , for various center-to-center separation distances (different curves). Each curve has fixed colloid center-to-center separation, as marked on the plot. (b) The cylinder separation angles with the greatest attraction or repulsion, as marked in (a). (c) Pair potential (plus an arbitrary uniform shift) for two cylinders held in the mirror-image single-particle-equilibrium orientations. (d) Two cylinders held in the mirror-image single-particle-equilibrium orientations with $\phi_{\text{sep}} = 90^\circ$, at center-to-center separations of (from left to right) 337.5, 315, and 292.5 nm. (e) Effect of sharpness parameter p on the effective interparticle force, at various center-to-center separations, linearly interpolated from free energy data. Left: cylinders with the same orientation and $\phi_{\text{sep}} = \tan^{-1}(a/b)$, the attractive direction identified in (a). Right: cylinders with mirror-image orientations and $\phi_{\text{sep}} = 90^\circ$. (f) A topologically entangled cylinder pair in a twist cell, with magenta arrows showing the rubbing directions at the top and bottom boundaries. Here the colloid diameter is 90 nm, the aspect ratio is $a/b = 1$, and $p = 10$.

the “S” profile with a “C” (Fig. 5d). Thereafter, the repulsion at separation angle $\phi_{\text{sep}} = 90^\circ$ is replaced with an attraction that strongly binds the two cylinders together. It is possible that such a switching move in an experiment would be followed by a reorientation of the cylinder to the opposite ground-state angle and a switch of the other end’s disclination kink to turn the “C” configuration back into an “S”, after which the cylinders could assemble end to end.

From the change in free energy with decreasing center-to-center separation distance at fixed ϕ_{sep} , we can infer the interparticle force along a specified separation direction. Fig. 5e shows these force calculations for three values of the superregg sharpness, $p = 4, 7$, and 10. For colloids with the same orientation, we consider separation along the attractive direction ϕ_{sep}

$= \phi_0 \approx \tan^{-1}(a/b)$ (left panel of Fig. 5e). For colloids in mirror-image configurations, we consider separation along $\phi_{\text{sep}} = 90^\circ$, along which the interaction changes from repulsive to attractive with decreasing distance (right panel of Fig. 5e). We find that the sign of the force is never changed by making the edges less sharp, as the qualitative features of the free energy’s dependence on the colloid separation vector do not change. However, decreasing p usually reduces the magnitude of the force. This reduction varies considerably, between 0% and 50% for $p = 7$ relative to $p = 10$, and between 17% and 87% for $p = 4$ relative to

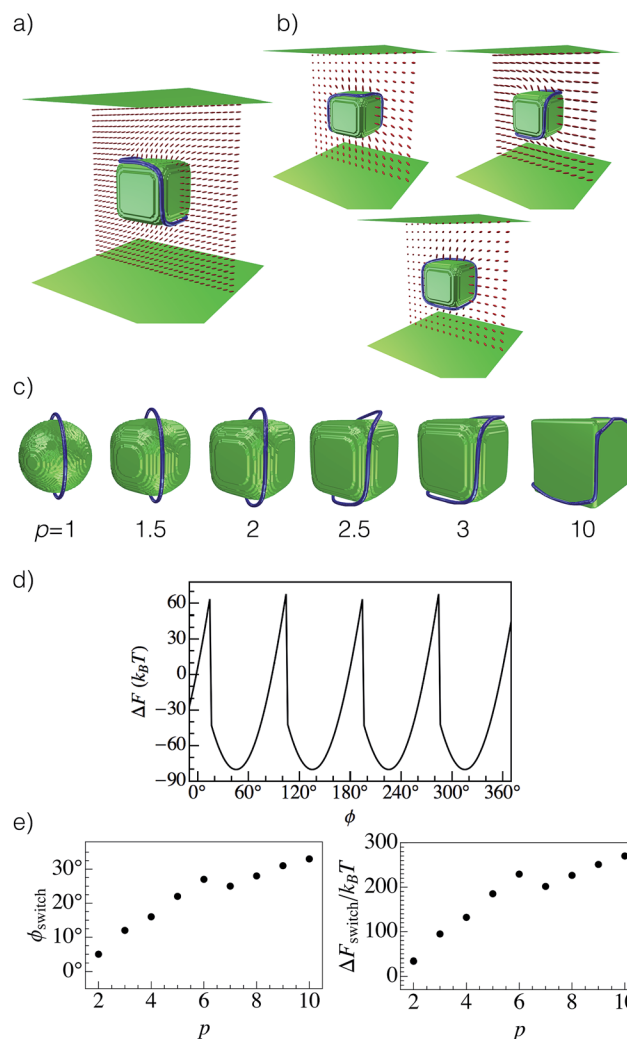


Fig. 6 Colloidal cubes. (a) The disclination follows the edges of the cube, enclosing three faces. (b) As the cube is rotated, the disclination cycles through four possible arrangements, that shown in (a) and the three shown here. (c) Superellipsoids of diameter 540 nm at various values of sharpness p , showing the gradual transformation of the disclination configuration. (d) Change in free energy as a cube is rotated about a vertical line through its center by angle ϕ , after numerically minimizing the energy with each incremental rotation. The cube is 180 nm on each side and is modeled as a superellipsoid with sharpness $p = 3$. (e) Colloid orientation angle ϕ_{switch} (modulo 90°) and magnitude of the change in free energy ΔF_{switch} when the disclination configuration suddenly switches, for superellipsoids of diameter 180 nm and varying sharpness p .

$p = 10$. Of the three tested values of p , the $p = 4$ superregg pair has the smallest-magnitude force at each value of ϕ_{sep} . This suggests that the sharpness of the colloidal particles' edges can be manipulated to change the strength of their interactions without altering the equilibrium configuration.

By changing the boundary conditions in the lateral directions to periodic, we can observe that cylinder chains repel one another laterally. This raises the possibility that, at high density, cylinders could self-organize into a one-dimensional lattice of tilted chains at a preferred spacing.

The fact that disclinations follow the sharp edges of cylinders also has implications for colloids' entanglement by merging of their disclinations. Such entanglement has drawn great interest for generating a variety of stable structures,⁷ including hierarchical assembly of colloids of different sizes⁴¹ and a wide array of defect knots and links in colloid lattices.⁸ A pair of entangled cylinders is shown in Fig. 5f, where a "twist cell" geometry with 90° offset between anchoring directions at the top and bottom surfaces is used to stabilize the entanglement. As with individual cylinders, the disclination travels in a straight line roughly along the long axis of the cylinder and then follows a portion of the sharp edge at the cylinder end before traversing to the end edge of the other cylinder.

4 Colloidal cubes

In going from ellipsoids to cylinders and microbullets, we found that adding an edge or two created a new realignment effect with significant consequences for colloidal assembly. What will happen if the colloids are cubical, with twelve edges? Now there exist many ways for a disclination to wrap around the colloid while following *only* edges.

We use LdG numerical modeling to study cubical colloids modeled using the special case of the superellipse equation, eqn (3), with two of the cube's faces having normals fixed in the vertical direction. The disclination now wraps around six of the colloid's twelve edges, dividing three faces from the other three, in one of the configurations shown in Fig. 6a and b. As with the rod-like colloids above, we rotate the cube about the z -axis to find the orientation that minimizes the free energy. We find that the cube prefers to have the normals of its side faces oriented at 45° relative to \vec{n}_0 .

As the sharpness p is varied, transforming a sphere continuously into an approximate cube, the disclination configuration also changes continuously, as shown in Fig. 6c. The vertical cube edges pin portions of the disclination, while above and below the cube the disclination deflects gradually toward the horizontal edges. The disclination also increasingly avoids cube vertices as p increases, because the nematic director profile around a disclination between two cube faces is incompatible with the normal direction of a third, mutually perpendicular cube face. As a result, for large values of p the disclination's otherwise straight contour is interrupted by deflections that conspicuously avoid the cube vertices, as shown in Fig. 6c for $p = 10$.

Hung and Bale³⁷ found numerically a similar defect configuration for smaller cubic nanoparticles of side length 40 nm in

certain orientations. However, for the cube orientations considered here, Hung and Bale found that the nematic melted over a large area of two or four cube faces, whereas all defects in our findings are line-like. The discrepancy likely arises from the earlier work's smaller cube size, closer to the nematic correlation length.

The multiplicity of possible disclination arrangements has a surprising consequence: sudden reconfiguration of the disclination ring when the cube is rotated. To see this, we conduct LdG energy minimization at an initial cube orientation, then rotate the cube by small increments, re-minimizing the energy after each increment. This models a quasi-static rotation of the colloid relative to fixed anchoring conditions at the top and bottom surfaces. The result, shown in Fig. 6d, is that the elastic free energy builds up until a sudden rearrangement of the disclination to a set of edges more compatible with the new cube orientation, allowing an abrupt drop in free energy. Upon further rotation, the cube keeps the same disclination arrangement through an energy minimum with ϕ at odd multiples of 45° before the elastic energy builds up again, leading to another sudden defect jump.

Changing the sharpness p of the superellipsoid used to approximate a cube quantitatively adjusts the cube orientation ϕ_{switch} at which this sudden switch in defect configuration occurs. Sharper edges more strongly pin the disclination, requiring a greater angle of rotation before the disclination rearrangement, and the resulting sudden drop in free energy ΔF_{switch} is of greater magnitude (Fig. 6e). Both ϕ_{switch} and ΔF_{switch} vary roughly linearly with p .

A similar but less drastic sudden defect reconfiguration also occurs for cylindrical colloids, between the two mirror-symmetric configurations mentioned previously.

Pair potentials for colloidal cubes were also calculated. As for pairs of cylinders above, the colloid orientations were fixed in the single-cube ground state, with the faces' normals at 45° angles to \vec{n}_0 . The interaction that we find here is simple but interesting: cubes attract face-to-face and repel edge-to-edge.

5 Summary and outlook

Through Landau-de Gennes numerical modeling of non-spherical homeotropic colloids, we have found that details of colloid shape, in particular the presence of sharp edges, have a remarkable effect in reshaping the companion disclination ring. The disclination executes sharp turns in order to follow (portions of) the edges so as to alleviate the elastic energy cost of splay required by strong homeotropic anchoring. While this might at first seem to be only a microscopic effect, the defect's attraction to edges leads to a realignment of the colloid relative to the background director field. The colloidal realignment in turn affects the geometry of colloidal assembly, as colloids tend to attract along the directions normal to the faces with sharp edges. This predicted realignment is in qualitative agreement with our experimental results and offers an explanation for previous experimental observations of oblique orientation of colloidal micro-rods.¹⁷ We also predict sudden changes in defect arrangement as the colloid is rotated relative to the far-

field director, or as colloids are forced together along a repulsive direction.

Our results suggest that it will be worthwhile to perform numerical and experimental studies on large numbers of sharp-edged colloids at high density. Self-assembled chains and lattices quite different from those formed by spheres could be produced and tuned by varying the colloids' geometrical parameters, such as aspect ratio and edge sharpness. Also, faceted colloid shapes of increased complexity could be investigated to determine the geometric possibilities offered by disclinations effectively confined to a one-dimensional subset of a three-dimensional system – a prospect that suggests exciting connections to topology.^{25,42} These areas of investigation will further the key finding presented here: colloidal assembly and alignment in nematic liquid crystals are highly sensitive to details of colloid shape, offering a route to tunable effective colloid interactions and an expanded library of self-assembly outcomes.

Note from the authors

Landau-de Gennes numerical modeling of cylindrical colloids in nematic liquid crystals has also been recently performed by S.M. Hashemi and M.R. Ejtehdi, arXiv:1410.1145 [cond-mat-soft]. Similar disclination configurations, as well as oblique colloid orientation depending on the aspect ratio, are observed in that work.

Acknowledgements

We thank Simon Čopar, Miha Ravnik, and Randall Kamien for helpful discussions. Our numerical LdG modeling benefited greatly from the advice and assistance of Gareth Alexander and Carl Goodrich. Most visualizations of numerical results were made using a POV-Ray scene file generator provided to us by Simon Čopar. This work was supported in part through the University of Pennsylvania MRSEC Grant NSF DMR11-20901. D.A.B. was supported by NSF Grant DGE-1321851 and by a University of Pennsylvania Teece Fellowship.

References

- 1 P. Poulin, H. Stark, T. Lubensky and D. Weitz, *Science*, 1997, **275**, 1770–1773.
- 2 I. Mušević, M. Škarabot, U. Tkalec, M. Ravnik and S. Žumer, *Science*, 2006, **313**, 954–958.
- 3 I. Smalyukh, S. Chernyshuk, B. Lev, A. Nych, U. Ognysta, V. Nazarenko and O. Lavrentovich, *Phys. Rev. Lett.*, 2004, **93**, 117801.
- 4 M. A. Gharbi, M. Nobili, M. In, G. Prévot, P. Galatola, J.-B. Fournier and C. Blanc, *Soft Matter*, 2011, **7**, 1467–1471.
- 5 M. Škarabot, M. Ravnik, S. Žumer, U. Tkalec, I. Poberaj, D. Babič, N. Osterman and I. Mušević, *Phys. Rev. E: Stat., Nonlinear, Soft Matter Phys.*, 2008, **77**, 031705.
- 6 E. Terentjev, *Phys. Rev. E: Stat. Phys., Plasmas, Fluids, Relat. Interdiscip. Top.*, 1995, **51**, 1330.
- 7 M. Ravnik, M. Škarabot, S. Žumer, U. Tkalec, I. Poberaj, D. Babič, N. Osterman and I. Mušević, *Phys. Rev. Lett.*, 2007, **99**, 247801.
- 8 U. Tkalec, M. Ravnik, S. Čopar, S. Žumer and I. Mušević, *Science*, 2011, **333**, 62–65.
- 9 A. Nych, U. Ognysta, M. Škarabot, M. Ravnik, S. Žumer and I. Mušević, *Nat. Commun.*, 2013, **4**, 1489.
- 10 I. Mušević, M. Škarabot and M. Humar, *J. Phys.: Condens. Matter*, 2011, **23**, 284112.
- 11 M. Ravnik, G. P. Alexander, J. M. Yeomans and S. Žumer, *Proc. Natl. Acad. Sci. U. S. A.*, 2011, **108**, 5188–5192.
- 12 P. F. Damasceno, M. Engel and S. C. Glotzer, *Science*, 2012, **337**, 453–457.
- 13 R. Ni, A. P. Gantapara, J. de Graaf, R. van Roij and M. Dijkstra, *Soft Matter*, 2012, **8**, 8826–8834.
- 14 J. de Graaf, R. van Roij and M. Dijkstra, *Phys. Rev. Lett.*, 2011, **107**, 155501.
- 15 L. Botto, E. P. Lewandowski, M. Cavallaro and K. J. Stebe, *Soft Matter*, 2012, **8**, 9957–9971.
- 16 K. J. Lee, J. Yoon and J. Lahann, *Curr. Opin. Colloid Interface Sci.*, 2011, **16**, 195–202.
- 17 U. Tkalec, M. Škarabot and I. Mušević, *Soft Matter*, 2008, **4**, 2402–2409.
- 18 F. R. Hung, *Phys. Rev. E: Stat., Nonlinear, Soft Matter Phys.*, 2009, **79**, 021705.
- 19 M. Tasinkevych, F. Mondiot, O. Mondain-Monval and J.-C. Loudet, *Soft Matter*, 2014, **10**, 2047–2058.
- 20 M. A. Gharbi, M. Cavallaro Jr, G. Wu, D. A. Beller, R. D. Kamien, S. Yang and K. J. Stebe, *Liq. Cryst.*, 2013, **40**, 1619–1627.
- 21 C. P. Lapointe, T. G. Mason and I. I. Smalyukh, *Science*, 2009, **326**, 1083–1086.
- 22 J. Dontabhaktuni, M. Ravnik and S. Žumer, *Soft Matter*, 2012, **8**, 1657–1663.
- 23 M. Cavallaro Jr, M. A. Gharbi, D. A. Beller, S. Čopar, Z. Shi, R. D. Kamien, S. Yang, T. Baumgart and K. J. Stebe, *Soft Matter*, 2013, **9**, 9099–9102.
- 24 B. Senyuk, Q. Liu, S. He, R. Kamien, R. Kusner, T. Lubensky and I. Smalyukh, *Nature*, 2012, **493**, 200–205.
- 25 T. Machon and G. P. Alexander, *Proc. Natl. Acad. Sci. U. S. A.*, 2013, **110**, 14174–14179.
- 26 M. Cavallaro, M. A. Gharbi, D. A. Beller, S. Čopar, Z. Shi, T. Baumgart, S. Yang, R. D. Kamien and K. J. Stebe, *Proc. Natl. Acad. Sci. U. S. A.*, 2013, **110**, 18804–18808.
- 27 N. M. Silvestre, Q. Liu, B. Senyuk, I. I. Smalyukh and M. Tasinkevych, *Phys. Rev. Lett.*, 2014, **112**, 225501.
- 28 Z. Eskandari, N. M. Silvestre, M. M. Telo da Gama and M. R. Ejtehadi, 2014, arXiv preprint, arXiv, 1406.0702.
- 29 C. Tsakonas, A. Davidson, C. Brown and N. Mottram, *Appl. Phys. Lett.*, 2007, **90**, 111913.
- 30 C. Luo, A. Majumdar and R. Erban, *Phys. Rev. E: Stat., Nonlinear, Soft Matter Phys.*, 2012, **85**, 061702.
- 31 M. Conradi, M. Ravnik, M. Bele, M. Zorko, S. Žumer and I. Mušević, *Soft Matter*, 2009, **5**, 3905–3912.
- 32 S. Čopar, M. Ravnik and S. Žumer, *Materials*, 2014, **7**, 4272–4281.
- 33 H. Stark, *Eur. Phys. J. B*, 1999, **10**, 311–321.

- 34 S. Grollau, N. Abbott and J. de Pablo, *Phys. Rev. E: Stat., Nonlinear, Soft Matter Phys.*, 2003, **67**, 011702.
- 35 M. Ravnik and S. Žumer, *Liq. Cryst.*, 2009, **36**, 1201–1214.
- 36 M. A. Gharbi, D. Seč, T. Lopez-Leon, M. Nobili, M. Ravnik, S. Žumer and C. Blanc, *Soft Matter*, 2013, **9**, 6911–6920.
- 37 F. Hung and S. Bale, *Mol. Simul.*, 2009, **35**, 822–834.
- 38 N. D. Mermin, *Rev. Mod. Phys.*, 1979, **51**, 591.
- 39 T. Lubensky, D. Pettey, N. Currier and H. Stark, *Phys. Rev. E: Stat. Phys., Plasmas, Fluids, Relat. Interdiscip. Top.*, 1998, **57**, 610.
- 40 J.-B. Fournier and P. Galatola, *Europhys. Lett.*, 2005, **72**, 403.
- 41 M. Škarabot, M. Ravnik, S. Žumer, U. Tkalec, I. Poberaj, D. Babič and I. Mušević, *Phys. Rev. E: Stat., Nonlinear, Soft Matter Phys.*, 2008, **77**, 061706.
- 42 S. Čopar, N. A. Clark, M. Ravnik and S. Žumer, *Soft Matter*, 2013, **9**, 8203–8209.